remote sensing

MDPI

Article

Hybrid Methodology Using Sentinel-1/Sentinel-2 for Soil Moisture Estimation

Simon Nativel [1], Emna Ayari [1,2,†], Nemesio Rodriguez-Fernandez [1], Nicolas Baghdadi [3], Remi Madelon [1], Clement Albergel [4] and Mehrez Zribi [1,*]

[1] CESBIO, CNES/CNRS/INRAE/IRD/UPS, Université de Toulouse, 18 Av. Edouard Belin, Bpi 2801, CEDEX 9, 31401 Toulouse, France; simon.nativel@univ-tlse3.fr (S.N.); emna.ayari@inat.u-carthage.tn (E.A.); nemesio.rodriguez-fernandez@univ-tlse3.fr (N.R.-F.); remi.madelon@univ-tlse3.fr (R.M.)
[2] National Agronomic Institute of Tunisia, Carthage University, Tunis 1082, Tunisia
[3] CIRAD, CNRS, INRAE, TETIS, University of Montpellier, AgroParisTech, CEDEX 5, 34093 Montpellier, France; nicolas.baghdadi@teledetection.fr
[4] European Space Agency Climate Office, ECSAT, Harwell Campus, Oxforshire, Didcot OX11 0FD, UK; Clement.albergel@esa.int
* Correspondence: mehrez.zribi@ird.fr; Tel.: +33-56155-8505
† LR17AGR01 InteGRatEd Management of Natural Resources: remoTE Sensing, Spatial Analysis and Modeling (GREEN-TEAM).

Abstract: Soil moisture is an essential parameter for a better understanding of water processes in the soil–vegetation–atmosphere continuum. Satellite synthetic aperture radar (SAR) is well suited for monitoring water content at fine spatial resolutions on the order of 1 km or higher. Several methodologies are often considered in the inversion of SAR signals: machine learning techniques, such as neural networks, empirical models and change detection methods. In this study, we propose two hybrid methodologies by improving a change detection approach with vegetation consideration or by combining a change detection approach together with a neural network algorithm. The methodology is based on Sentinel-1 and Sentinel-2 data with the use of numerous metrics, including vertical–vertical (VV) and vertical–horizontal (VH) polarization radar signals, the classical change detection surface soil moisture (SSM) index I_{SSM}, radar incidence angle, normalized difference vegetation index (*NDVI*) optical index, and the VH/VV ratio. Those approaches are tested using in situ data from the ISMN (International Soil Moisture Network) with observations covering different climatic contexts. The results show an improvement in soil moisture estimations using the hybrid algorithms, in particular the change detection with the neural network one, for which the correlation increases by 54% and 33% with respect to that of the neural network or change detection alone, respectively.

Keywords: soil moisture; Sentinel-1; Sentinel-2; change detection; artificial neural network

Citation: Nativel, S.; Ayari, E.; Rodriguez-Fernandez, N.; Baghdadi, N.; Madelon, R.; Albergel, C.; Zribi, M. Hybrid Methodology Using Sentinel-1/Sentinel-2 for Soil Moisture Estimation. *Remote Sens.* **2022**, *14*, 2434. https://doi.org/10.3390/rs14102434

Academic Editors: Wei Zhao, Jian Peng, Hongliang Ma, Chunfeng Ma and Jiangyuan Zeng

Received: 7 April 2022
Accepted: 17 May 2022
Published: 19 May 2022

1. Introduction

Soil moisture is a key parameter for understanding different processes related to the transfer of the soil–vegetation–atmosphere flux [1–3]. It is also an essential parameter in the management of water resources, particularly for optimizing irrigation [4,5]. In this context, remote sensing has greatly contributed to allowing the spatial and temporal monitoring of this parameter at different spatial scales from global to local [6,7].

Most of the currently available operational surface soil moisture products are on a global scale with spatial resolutions of several kilometers. They are essentially based on active and passive microwave measurements [8–12]. In passive microwaves, these are mainly products based on SMOS [8] and SMAP [9] missions dedicated to monitoring soil moisture with L-Band measurements and other non-dedicated sensors using higher frequency bands. In active microwaves, these are measurements based on acquisitions with

a scatterometer, particularly data acquired by the ASCAT/METOP satellite series [13]. The European Space Agency (ESA) Climate Change Initiative (CCI) soil moisture project also provides long time series by merging soil moisture estimations from active and passive sensors [14].

For soil moisture estimation at high spatial resolution, we identify products with an average resolution at approximately 1 km or at the plot scale [15–24]. There have been various studies that have developed methodologies based on low-resolution data disaggregation techniques, notably with measurements acquired in thermal infrared (MODIS) [25] or, more recently, data acquired by SAR sensors. The Synthetic Aperture Radar (SAR) technique offers a high spatial resolution estimate of the radar signal adapted to applications at agricultural field scale. The measured signal is dependent on the radar configurations (frequency, incidence angle, and polarization) and the dielectric and geometric properties of the surface. After numerous demonstration space missions (ERS, ASAR/ENVISAT, RADARSAT, etc.), the arrival of Sentinel-1 constellation [26] in the context of the Copernicus program has enabled exponential growth in the use of these signals for monitoring soil moisture and the dynamics of the vegetation cover. Other soil moisture products are then offered only based on Sentinel-1 data, with three types of methodologies: one based on the direct inversion of physical or semiempirical models [27–29]; one based on the application of machine learning approaches and particularly neural networks [30–32]; and one based on the change detection technique [33–35]. For example, at plot scale, El Hajj et al. [31] presented an Artificial Neural Network (ANN) approach with training using the coupling of the Integral Equation Model (IEM) and the Water Cloud Model (WCM) to provide an estimate of soil moisture at the scale of the agricultural plot. Gao et al. [35] also proposed an approach at the plot scale with greater consideration of the vegetation cover and its effect on the temporal variation of the radar signal. Bauer-Marschallinger et al. [33] proposed a change detection approach very close to the initial approach proposed with data from ASCAT scatterometers [13] at a 1 km scale.

For these products, which are highly useful for regional hydrology, the validation of existing products, despite the very interesting potential, still shows some limitations in different contexts, in particular that of dense vegetation covers but also in relatively complex contexts with strong heterogeneities in terms of land use and topography [36].

In this context, this study proposes to test hybrid approaches to soil moisture retrieval at a 1 km scale with the objective of improving the estimation accuracy of soil moisture. The approaches consider hybrid methodologies with a combination of a change detection approach with empirical modeling or machine learning.

Section 2 presents in the first subsection the database used in this study in terms of soil moisture data and satellite measurements. The second subsection presents the methodologies tested and proposed in this study. Section 3 illustrates the results. Section 4 includes the discussion of the proposed applications. The conclusions are presented in Section 5.

2. Materials and Methods

2.1. Database

2.1.1. ISMN Soil Moisture Data

The training and validation of the proposed methods are conducted based on data from the International Soil Moisture Network (ISMN) [37]. The data are available in conjunction with additional datasets of Koppen–Geiger climate classes, ESA's CCI land cover, and soil characteristics. The upper soil layer (0–10 cm) moisture measurements are harmonized as fractional volumetric soil moisture (m^3/m^3) and converted into Coordinated Universal Time (UTC). After data quality verification, some ISMN networks suffer from a lack of measurements. Therefore, we considered 21 networks among a total of 71 spatially distributed as shown in Figure 1. The data of each station should cover a period of two years with at least 20 dates between the start and the end date of acquisitions—1 January 2015 and 19 August 2021, respectively. Consequently, in the same network, we retain only stations with valid dataset as detailed in Table 1.

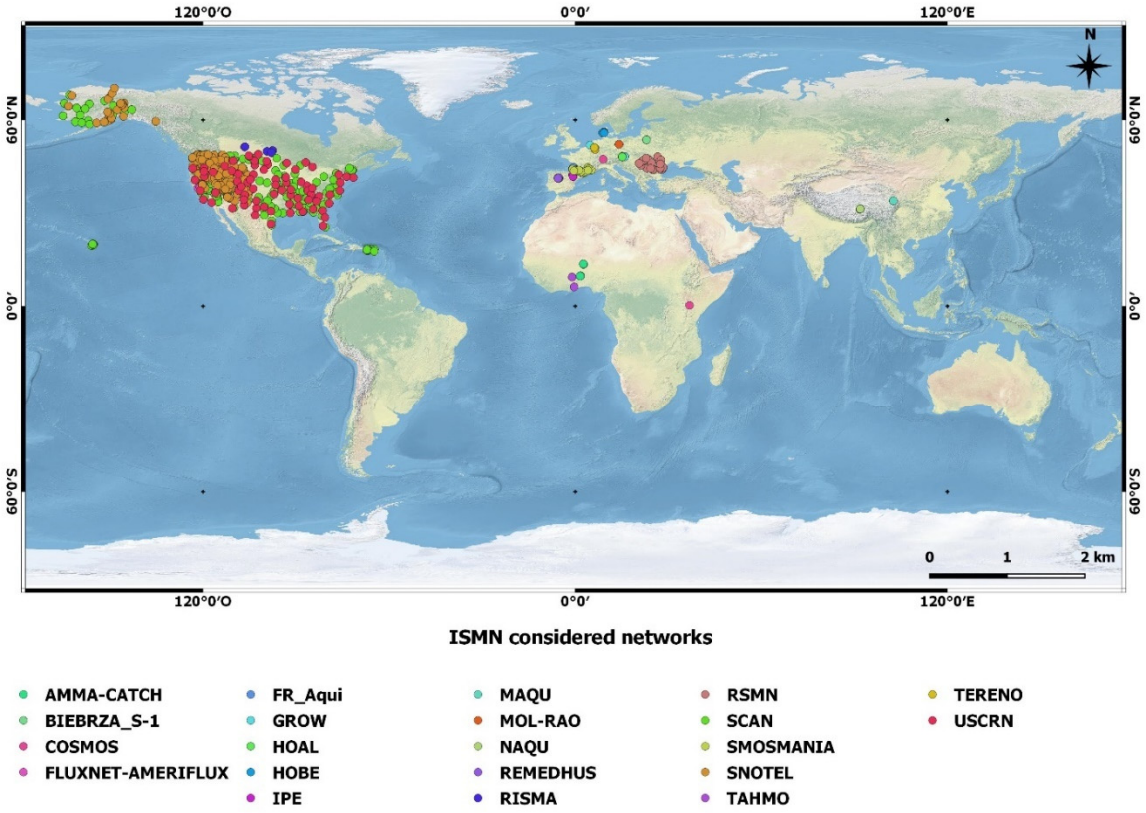

Figure 1. The global distribution of the International Soil Moisture Network (ISMN).

Table 1. Overview of the considered ISMN networks.

Network	Country	Number of Selected Stations	SM Sensors	References
AMMA-CATCH	Benin, Niger	7	CS616	Cappelaere et al. [38]; De Rosnay et al. [39]; Lebel et al. [40]; Mougin et al. [41]; Pellarin et al. [42]; Galle et al. [43].
BIEBRZA-S-1	Poland	8	GS-3	Musial et al. 2016 [44]
COSMOS	USA	2	Cosmic-ray-Probe	Zreda et al. [45]; Zreda et al. [46]
HOBE	Denmark	3	Decagon-5TE	Bircher et al. [47]; Jensen et al. [48]
FLUXNET-AMERIFLUX	USA	4	CS655, ThetaProbe-ML3 ThetaProbe-ML2X,	
FR-Aqui	France	3	ThetaProbe ML2X	Al-Yaari et al. [49]; Wigneron et al. [50]
GROW	UK	20	Flower-Power	Zappa et al. [51]; Xaver et al. [52]; Zappa et al. 2020 [53]
HOAL	Austria	32	SPADE-Time-Domain-Transmissivity	Vreugdenhil M. et al. [54]; Blöschl, Günter, et al. [55]
IPE	Spain	2	CS655, ThetaProbe-ML2X	Alday et al. [56]

Table 1. *Cont.*

Network	Country	Number of Selected Stations	SM Sensors	References
MAQU	China	1	ECH20-EC-TM	Su et al. [57]; Dente et al. [58]
MOL-RAO	Germany	1	TRIME-EZ	Beyrich F. and Adam W.K. [59]
NAQU	China	5	5TM	Su et al. 2011 [60]
REMEDHUS	Spain	13	Stevens-Hydra-Probe	Gonzalez-Zamora et al. [61]
RISMA	Canada	5	Hydraprobe-II-Sdi-12	Canisius F. [62]; L'Heureux J. [63]; Ojo et al. [64]
RSMN	Romania	19	5TM	
SCAN	USA	130	Hydraprobe-Sdi-12/Ana	Schaefer et al. [65]
SMOSMANIA	France	15	ThetaProbe ML2X	Calvet et al. [66]; Albergel et al. [67]; Calvet et al. [68]
SNOTEL	USA	84	Hydraprobe-Analog-(2.5-Volt)	Leavesley et al. [69]
TAHMO	Ghana	3	TEROS10, TEROS12	
TERENO	Poland	4	Hydraprobe-II-Sdi-12	Zacharias et al. [70]; Bogena et al. [71]; Bogena et al. [72]
USCRN	USA	77	Stevens-Hydraprobe-II-Sdi-12	Bell et al. [73]

2.1.2. Sentinel-1

The first S-1A satellite was launched on 3 April 2014 and was followed by the S-1B Sentinel satellite on 25 April 2016. This dual-satellite constellation offers a 6-day repeat frequency for all regions of the globe [74]. The SAR payloads use a C-band frequency of 5.4 GHz and have the following standard operating modes: stripe map (SM), interferometric wide swath (IW), extra wide swath (EW), and WaVe (WV). In the present study, IW S-1 images are analyzed. They are characterized by a 10 m × 10 m spatial resolution and dual VV and VH polarization measurements. All of the images were generated from the high-resolution, Level-1 Ground Range Detected (GRD) product. The calibration is designed to convert the digital values of the raw images into backscattering coefficients (σ0).

2.1.3. Sentinel-2

After the launch of Sentinel-2 A and B on 23 June 2015 and 7 March 2017, respectively, optical data became free and open access with a spatial resolution varying between 10 m × 10 m and 60 m × 60 m and a revisit time of up to 5 days in 13 spectral bands at visible and mid-infrared wavelengths. In the present study, we used Sentinel-2 surface reflectance products downloaded from the Theia site (https://www.theia-land.fr/, accessed on 16 May 2022), already orthorectified and atmospherically corrected with a mask of clouds and shadows owing to the MAJA algorithm [75]. On each acquisition date and using red visible and near infrared bands with center wavelengths of approximately 665 and 833 nm, respectively, we calculated the Normalized Difference Vegetation Index ($NDVI$) and averaged this index for each studied station as expressed in the following equation:

$$NDVI = \frac{R_{NIR} - R_{Red}}{R_{NIR} + R_{Red}} \quad (1)$$

where R_{NIR} and R_{Red} are the surface reflectance in the two bands, near infrared and red visible, respectively.

2.1.4. Satellite Data Processing

Both radar backscattering coefficients and *NDVI* time series are identified at each station. A temporal linear interpolation of *NDVI* data is proposed to estimate the *NDVI* at each radar acquisition date. In this averaging, a filter is applied to the optical pixels to only consider data between 0.15 and 0.8 of *NDVI* to avoid urban areas and water covers with low *NDVI* or strong *NDVI* corresponding mainly to dense forests.

The radar signal is averaged over a radius of 500 m around each station. For a given station, if more than 50% of the Sentinel-1 pixels are excluded, the processing of radar data is not considered for the analyzed data.

2.2. Methodology

2.2.1. Change Detection Algorithm

The classic change detection *SSM* index I_{SSM} is defined as [76]:

$$I_{SSM} = \frac{SSM_t - SSM_{min}}{SSM_{max} - SSM_{min}} = \frac{\sigma_{VV} - \sigma_{VVmin}}{\sigma_{VVmax} - \sigma_{VVmin}} \quad (2)$$

where SSM_t is the soil moisture content at time t; SSM_{min} and SSM_{max} are the minimum and maximum values of in situ soil moisture, respectively; σ_{VV} is the radar signal at time t; and σ_{VVmin} and σ_{VVmax} are the minimum and maximum values of the radar signal time series, respectively. An index equal to 1 corresponds to the wettest context, and an index equal to 0 corresponds to the driest context.

To convert this index I_{SSM} to volumetric soil moisture at time t SSM_t, we introduce [77]:

$$SSM_t = I_{SSM} \times (SSM_{max} - SSM_{min}) + SSM_{min} \quad (3)$$

2.2.2. Improved Change Detection Approach

For the classic detection approach, radar signal change is linked to soil moisture change. It can be written as:

$$\Delta_{VV} = \alpha \, \Delta_{SSM} \quad (4)$$

where the soil moisture changes and the radar signal change in VV polarization are expressed in Equations (5) and (6), respectively.

$$\Delta_{SSM} = SSM_t - SSM_{min} \quad (5)$$

$$\Delta_{VV} = \sigma_{VV} - \sigma_{VVmin} \quad (6)$$

This relationship is adapted from [35,78]. It considers as a hypothesis that the difference between two radar signals acquired on two different dates is mainly related to the change in the hydric state of the soil.

Here, we propose an improved change detection methodology by using a hybrid change detection and empirical approach in which the effect of the vegetation is taken into account thanks to a vegetation-related variable $V1$. Using this approach, the radar signal change is related to the soil moisture change by the following expression:

$$\Delta_{VV} = (\alpha - \beta \, V1) \, \Delta_{SSM} \quad (7)$$

Unlike forward modeling approaches such as the WCM, the radar signal and the soil moisture are introduced as the difference between the radar signal at time t and the minimum signal corresponding to the minimum moisture and the difference between the soil moisture and the minimum moisture value, respectively.

The main objective of introducing the change as a function of time is to reduce the dependency to other variables affecting the radar signal such as soil roughness, which can be very important, particularly in the context of strong topography or even important spatial changes in microtopography, that change little with time for a given site, in contrast to soil moisture. Two vegetation-related quantities were tested for the $V1$ parameter: the optical vegetation index *NDVI* estimated from Sentinel-2 data, as illustrated in Section 2.3, and the VH/VV ratio, considered to be strongly linked to the dynamics of the vegetation cover. This second option could be particularly interesting in the context of a humid climate with limited optical data.

2.2.3. Artificial Neural Network Hybrid Approach

The multilayer perceptron (MLP), which is a multilayer feed-forward ANN, is one of the most widely used ANNs, mainly in the field of water resources [79,80]. A multilayer perceptron has one or more hidden layers between its input and output layers. The neurons are organized in layers such that neurons of the same layer are not interconnected and that the connections are directed from lower to upper layers. Each neuron returns an output based on a weighted sum of all inputs and according to a nonlinear function called the transfer or activation function. The input layer, made up of different metrics from Sentinel-1 and Sentinel-2 data, is connected to the hidden layer(s), which is made up of hidden neurons. The final estimates of the ANN are given by an activation function associated with the final layer called the output layer, using a sum of the weighted outputs of the hidden neurons.

The ANN model architecture consists of three hidden layers of 20 neurons with a rectified linear function (ReLu) as activation functions and an output layer with a single neuron with a linear activation function. The mean square error was used as the loss function and the gradient backpropagation was carried out using a first order stochastic gradient-based optimizer (Adam).

Different predictors based on Sentinel-1 and Sentinel-2 were tested to estimate soil moisture: VV, VH, incidence angle, VH/VV, *NDVI*, and I_{SSM}.

1. The VV and VH signals are identified for their high sensitivity to soil moisture.
2. The classical change detection *SSM* index I_{SSM} is calculated as a function of radar backscattering coefficients in VV polarization to use it for soil moisture estimation.
3. The incidence angle has an effect on the contribution of soil and vegetation components on the radar signal.
4. The *NDVI* index is identified to take into account the effect of vegetation cover on the backscattering signal.
5. The VH/VV ratio is identified to take into account the effect of vegetation cover on the backscattering signal [81].
6. SSM_t estimated from the classic change detection approach described in Section 3.1, Equation (2) is also considered as input.

The ANN models were trained using in situ soil moisture measurements retrieved from the ISMN as target. The training of the ANN models was conducted using 70% of the data samples. Thirty percent were kept for validation.

2.3. Statistical Parameters for Accuracy Assessment

Datasets are randomly subdivided into two parts: 70% of the database for model calibration and 30% for validation. The training data are used to calculate the different parameters to be estimated in the empirical and semiempirical models.

The *Bias*, root mean square error (*RMSE*) and Pearson's correlation (R) are considered to estimate the precision of the models.

$$Bias = P_i^{estimated} - P_i^{measured} \quad (8)$$

$$RMSE = \sqrt{\frac{1}{N}\sum_{i=1}^{N}\left(P_i^{estimated} - P_i^{measured}\right)^2} \quad (9)$$

where N is the number of data samples, $P_i^{estimated}$ is the estimated value of sample i, and $P_i^{measured}$ is the measured value of sample i.

$$R = \frac{\sum_{i=1}^{N}(x_i - \overline{x})(y_i - \overline{y})}{\sqrt{\sum_{i=1}^{N}(x_i - \overline{x})^2}\sqrt{\sum_{i=1}^{N}(y_i - \overline{y})^2}} \quad (10)$$

where x_i and y_i are individual samples taken at points indexed with the variable i.

3. Results

3.1. Improved Change Detection Approach

The empirical improved change detection approach has a double objective, taking into account the effect of vegetation and limiting the effect of surface geometry. The calibration of α and β parameters were conducted by using 70% of the dataset selected randomly (23869 samples). For the validation, the remaining 10,229 samples of the dataset were used.

Figure 2 illustrate the validations of the different algorithms described in Section 3.2 tested with ISMN data. The proposed results show an improvement in accuracy by considering the effect of vegetation cover in the tested relationships. The *RMSE* (*R*) values decrease (increase) from 0.074 m^3/m^3 (0.58) from the change detection approach (Equation (2), Figure 2a) to 0.073 m^3/m^3 (0.59) for the improved change detection approach (Equation (7)) when the VH/VV ratio is used as the V1 parameter and to 0.068 m^3/m^3 (0.63) when NDVI is used as the *V1* (Figure 2b).

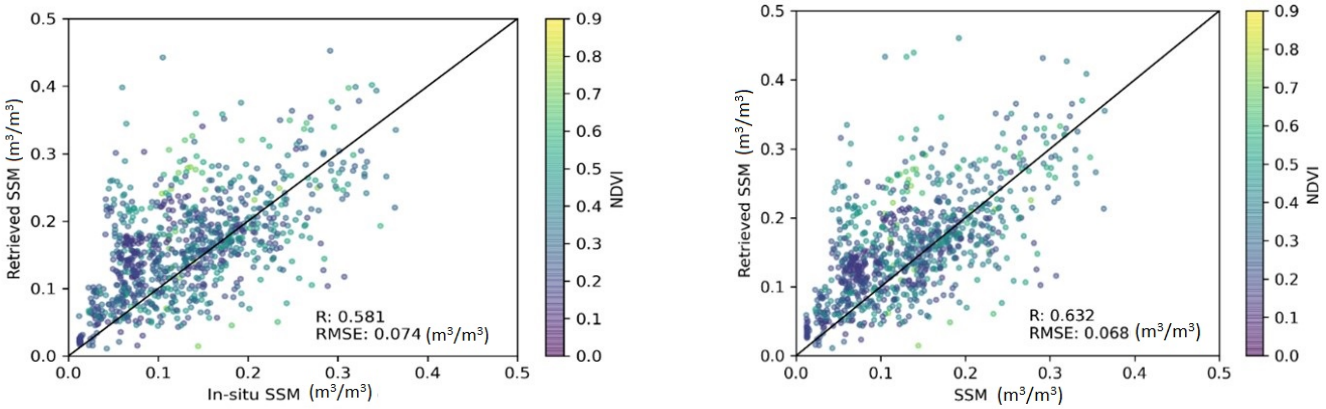

Figure 2. Scatterplots of the retrieved surface soil moisture (SSM) as a function of in situ SSM measurements colored according to NDVI value variation using two change detection approaches: (**a**) classic approach and (**b**) new approach expressed in Equation (7), where *V1* is the *NDVI*.

3.2. Neural Network Hybrid Approach

The different combinations of input metrics are tested to estimate soil moisture. Figure 3 illustrates the results of validations applied for 30% of the database, for each case of combination with the statistical parameters *RMSE* and *R*.

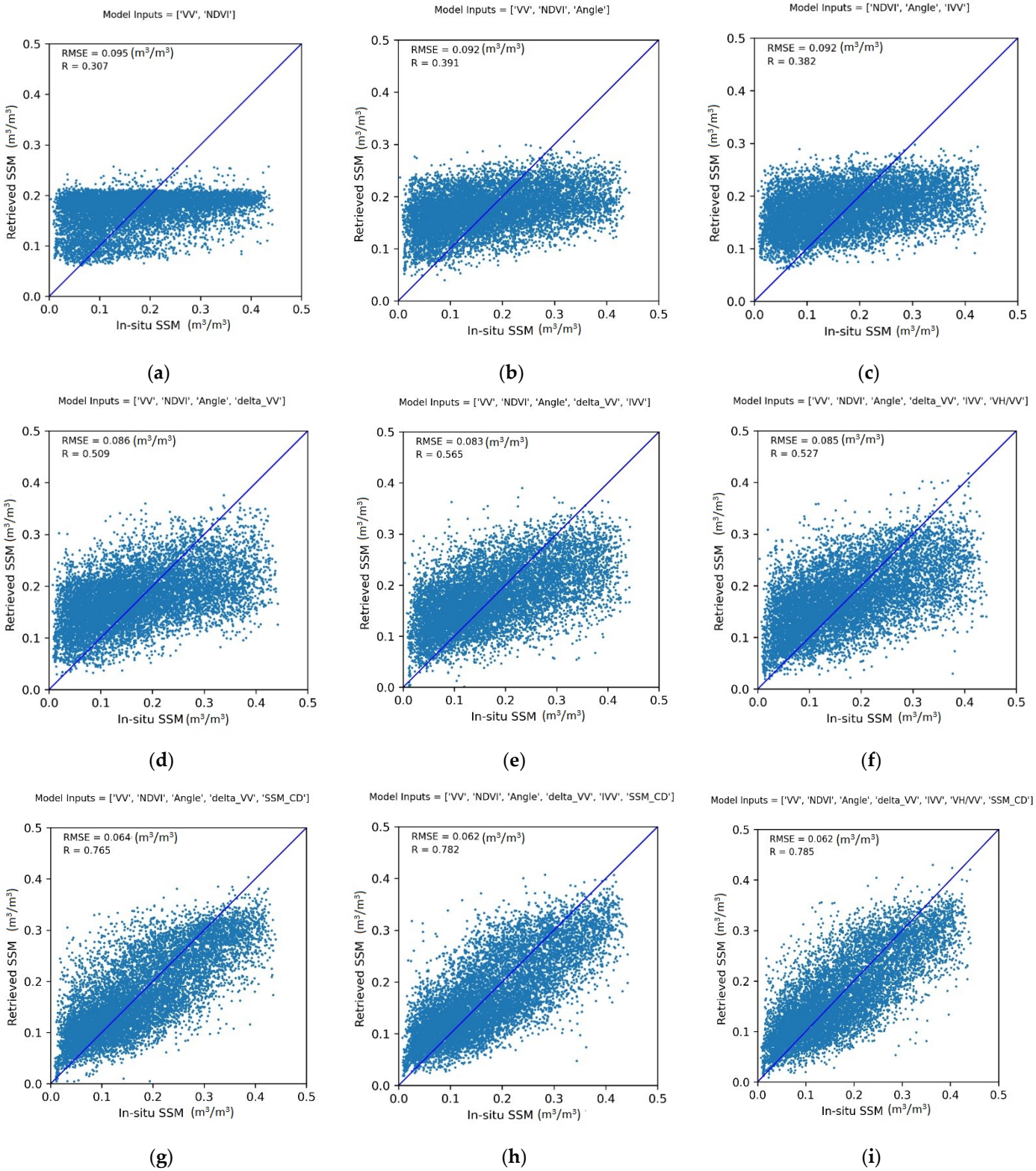

Figure 3. Scatterplots of the retrieved SSM as a function of in situ SSM measurements using the ANN approach using multiple combinations of features: (**a**) VV, *NDVI*, (**b**) VV, *NDVI*, the incidence angle, (**c**) *NDVI*, the incidence angle, I_{SSM}, (**d**) VV, *NDVI*, the incidence angle, Δ_{VV}, (**e**) VV, *NDVI*, the incidence angle, Δ_{VV}, I_{SSM}, (**f**) VV, NDVI, the incidence angle, Δ_{VV}, I_{SSM}, VH/VV ratio, (**g**) VV, *NDVI*, the incidence angle, Δ_{VV}, SSM_t, (**h**) VV, *NDVI*, the incidence angle, Δ_{VV}, I_{SSM}, SSM_t, (**i**) VV, *NDVI*, the incidence angle, Δ_{VV}, I_{SSM}, VH/VV ratio, SSM_t.

For the first six predictor combinations (Figure 3a–f), we observe relatively close precision with *RMSE* values in the range of 0.095 m^3/m^3 and 0.083 m^3/m^3 and *R* of 0.3–0.6. The introduction of moisture estimated by the classic change detection algorithm (Equation (3)) as input to ANN allows a strong improvement in the accuracy of soil moisture estimation with an *RMSE* equal to 0.063 m^3/m^3 and $R = 0.76$ when we consider the predictors: VV, *NDVI*, the incidence angle, Δ_{VV}, and SSM_t. By adding the VH/VV ratio and I_{SSM}, the *RMSE* value decreases to 0.062 m^3/m^3, and the correlation coefficient reaches a value of approximately 0.79. This result confirms the contribution of the hybrid approach to estimating soil moisture. This first estimated soil moisture strongly contributes to a better estimate of soil moisture by the ANN.

Figure 4 illustrates the accuracy of intercomparisons between in situ measurements and satellite estimates for the optimal case for different tested networks, where we represent the *RMSE* and *R* parameters by blue and orange boxes. The *RMSE* values vary from 0.03 m^3/m^3 to 0.09 m^3/m^3, and *R*-values fluctuate between 0.37 and 0.84.

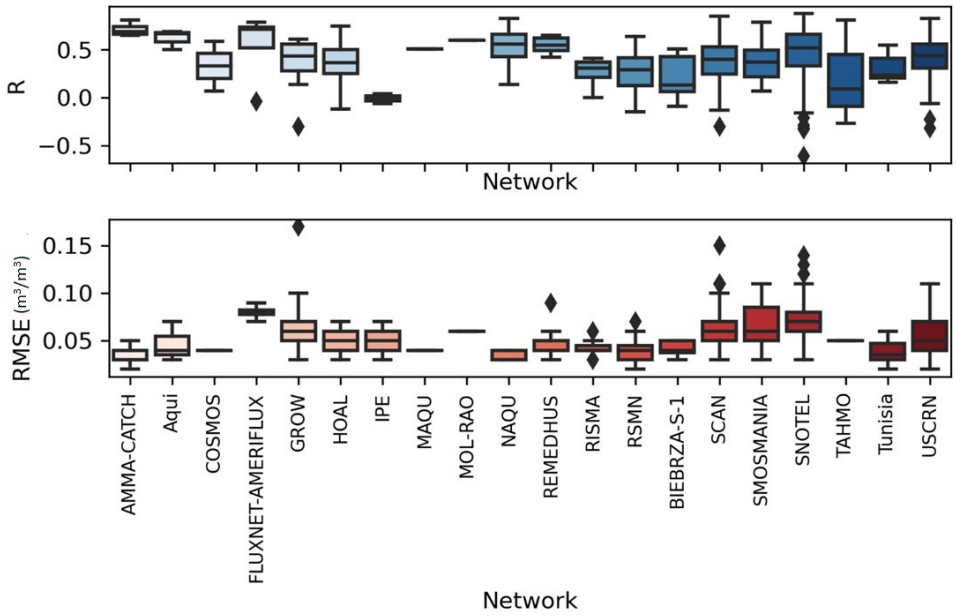

Figure 4. Boxplots of statistical parameters (*R* and *RMSE*) of soil moisture retrieval as a function of ISMN-considered networks using the hybrid methodology of change detection and ANN.

Good consistency is generally observed for networks such as AMMA-CATCH, COSMOS, MAQU, RSMN, HOAL, HOBE, IPE, BIEBRZA S-1, TAHMO, REMEDHUS and RISMA, and *RMSE* values are under or equal to 0.05 m^3/m^3. The NAQU network is characterized by the lowest *RMSE* value of 0.03 m^3/m^3 and *R* value of 0.77.

Within the same soil moisture in situ network, the accuracy of soil moisture retrieval varies from one station to another. For the REMEHDUS case characterized by an *RMSE* equal to 0.05 m^3/m^3, *RMSE* values per station range between 0.03 m^3/m^3 and 0.09 m^3/m^3, and R values vary between 0.34 and 0.69, as represented in Figure 5.

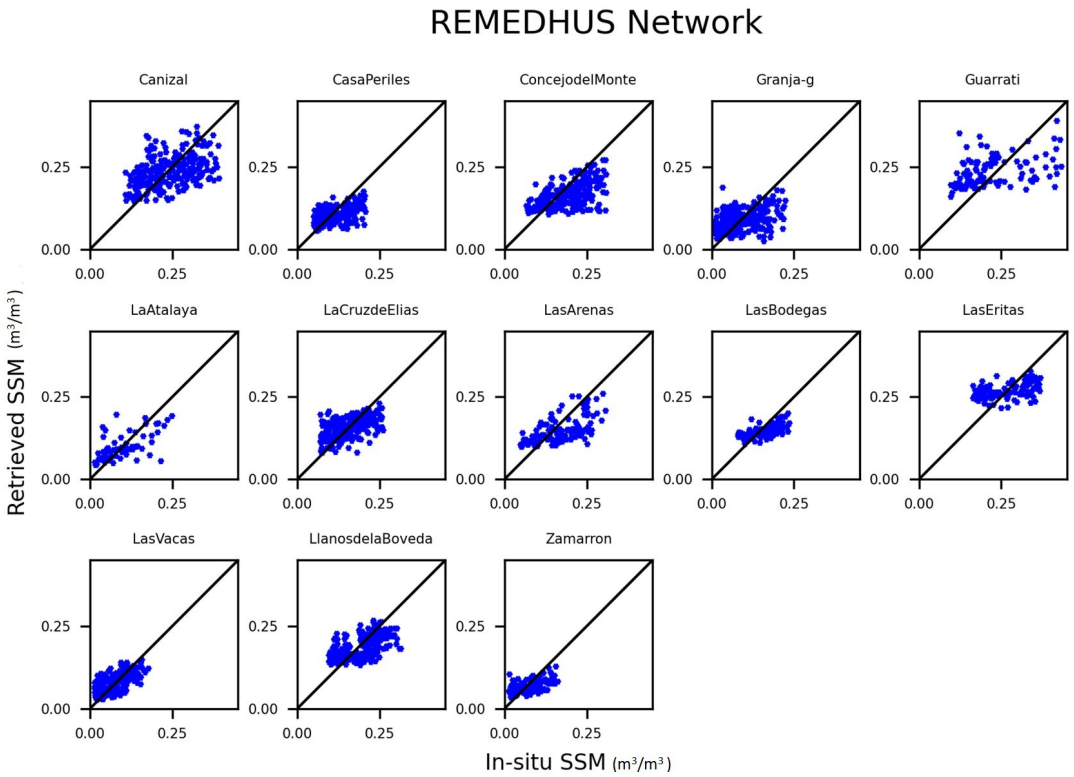

Figure 5. Scatterplots of the estimated soil moisture as a function of ISMN measurements in the REMEDHUS network per considered station.

4. Discussion

The proposed hybrid approaches have allowed more or less strong improvements compared to the initial estimates based on change detection or a separate ANN approach. With an improved change detection method, we observe a negligible contribution of the considered vegetation cover compared to a basic approach directly linking the radar signal to soil moisture. This can be explained by the highly diversified context at the scale of many soil moisture stations with very varied landscape contexts (crops, trees, bare soils, etc.) and different vegetation densities, which can generate significant noise in the modeling of the scattered signal that is difficult to take into account without a more precise description in terms of land use. This noise is particularly observed with the VH/VV index, which is very sensitive to the dynamics of the vegetation cover in a homogeneous context [81], but it could also mix different effects and particularly those of soil roughness [82].

To better analyze proposed results, we examined the time series of the in situ and retrieved soil moisture per station and network. Figure 6 displays the time series of the radar signal (VV), *NDVI*, and soil moisture SSM_t. The in situ soil moisture measurements are illustrated in blue, and the hybrid approach results are drawn in red. The intercomparison between the proposed approach performance within the LasBodegas and Canizal stations reveals *RMSE* values of 0.04 m^3/m^3 and 0.07 m^3/m^3, respectively. The two stations belong to the same climatic region of the arid steppe and characterize a clay fraction interval of approximately 35%. The performance difference may be induced by the land cover, where the Canizal station is occupied by shrubs and the LasBodegas station is covered by trees. The aforementioned land cover may impact the accuracy of soil moisture retrieval due to the vegetation volume impact on the radar signal in the C-band. Additionally, the measured soil moisture values are lower than 0.3 m^3/m^3 at the LasBodegas station, and higher values reach 0.4 m^3/m^3 at the Canizal station. Hence, the soil water content retrieval is more accurate in the first case due to the saturation of the C-band signal at high values of soil moisture.

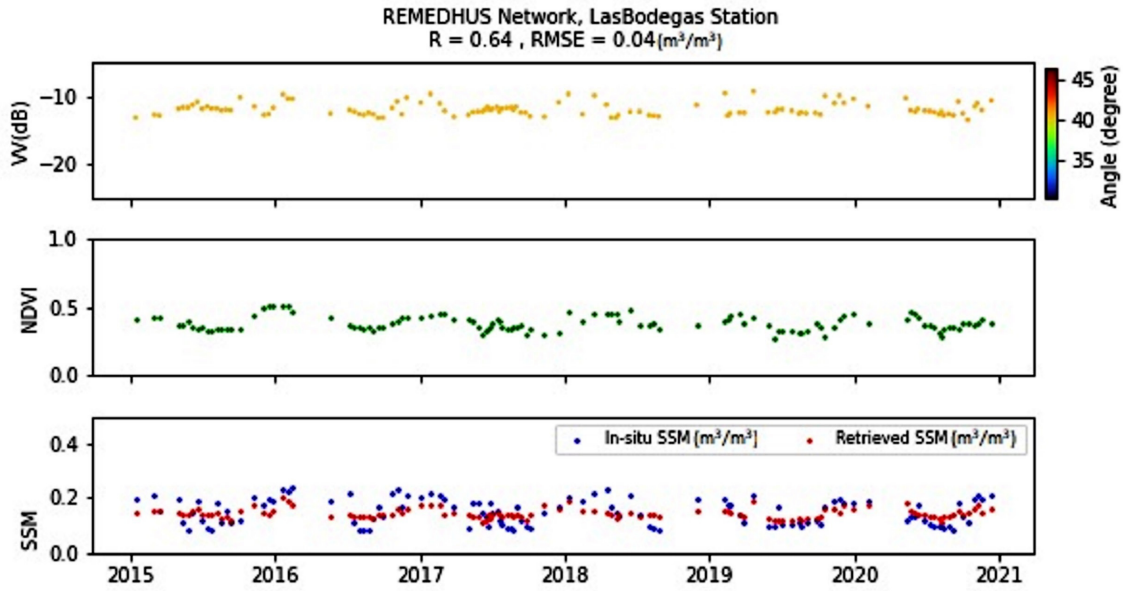

(**a**)

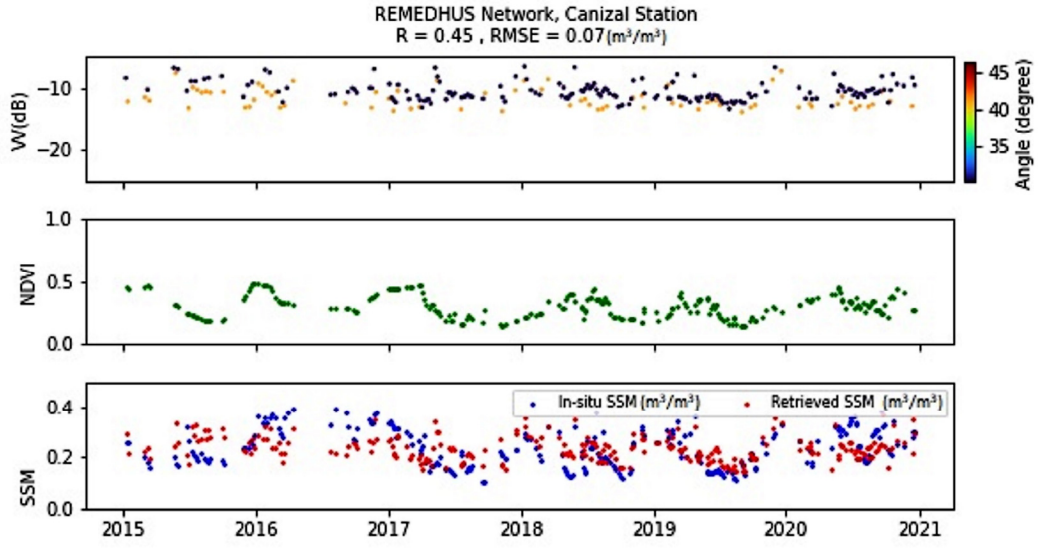

(**b**)

Figure 6. Scatterplots of the temporal evolution of radar signals in VV polarization, NDVI, and the predicted and in situ measurements of soil moisture using the hybrid methods within two stations of the REMEHDUS network: (**a**) LasBodegas station, (**b**) Canizal station.

However, the approach has difficulties for certain stations, as shown for FLUXNET-AMERFLUX, GROW, SNOTAL, and SMOSMANIA networks, where the *RMSE* values reach a maximum of 0.09 m^3/m^3. The analysis of these cases generally leads to contexts of dense vegetation cover that can induce a low sensitivity of the radar signal to soil moisture.

In Figure 7, we scatterplot the statistical parameters as a function of *NDVI* values. According to Figure 7a,b, we observe the increase of *RMSE* and *Bias* values as a function of the increase of *NDVI* values where *RMSE* can reach 0.10 m^3/m^3. The vegetation development may induce a *Bias* between -0.06 m^3/m^3 and 0.04 m^3/m^3, where *NDVI* values exceed 0.5. This behavior may be explained by the C-band potential which is otherwise limited in dense canopies where *NDVI* values are higher than 0.5.

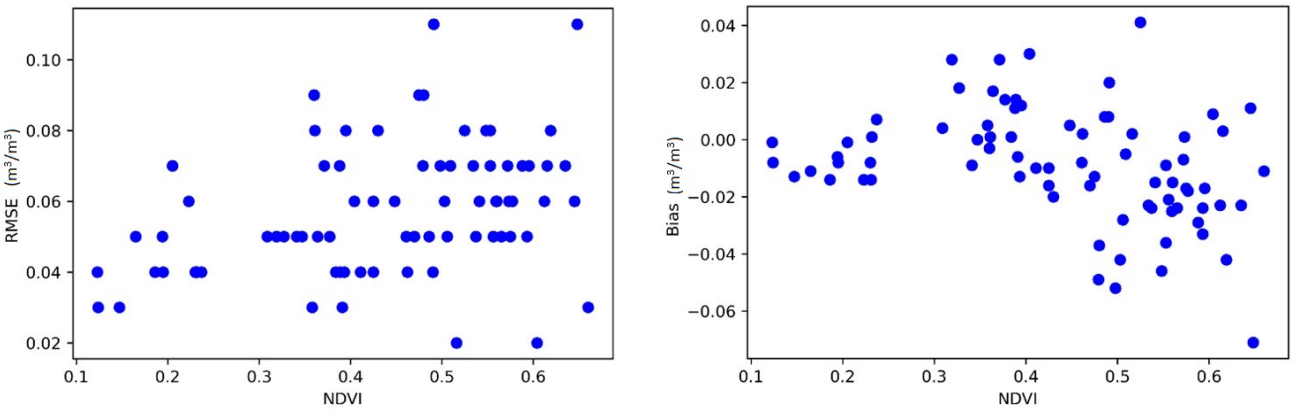

(**a**) (**b**)

Figure 7. Scatterplots of statistical parameters of the hybrid approach performance to retrieve SSM as a function of *NDVI* values stations: (**a**) *RMSE*, (**b**) *Bias*.

This is difficult to take into account in a general approach based on a neural network trained on stations with different types of surface conditions, such as the case of the FLUXNET-AMERFLUX network. The station land covers are a mixture of grasslands, temporary crops followed by harvest and bare soil periods, and woody savanna characterized by forest canopy cover between 30% and 60% and vegetation height exceeding 2 m. In this land cover context, the vegetation volume impacts the radar signal and complicates the soil moisture retrieval. We observe the vegetation impact within many stations in the SMOSMANIA network, such as the Mazan-Abbaye, Cabriers Avignon, and Ville Vieille stations occupied by trees or shrubs.

Furthermore, the use of *NDVI* as a vegetation descriptor may induce other limits, such as the availability of data in regions with temperate climates. The presence of clouds contaminates the surface reflectance, which damages the radiometric information. As a result, many time series suffer from gaps and lack data, which complicates the training and validation of the proposed model, such as the case of some stations of the USCRN network, where the mean *RMSE* value is equal to 0.06 m^3/m^3.

By considering the GROW network data, the *RMSE* is equal to 0.07 m^3/m^3. This relatively low accuracy in retrieving soil moisture may be linked to the predominant cold climate of the considered stations. This low-temperature climate may impact the radar signal, especially with the freeze–thaw phenomenon. This change in the physical state of the soil water content generates a fast variability in the Sentinel-1 signal, as discussed for agricultural plots in metropolitan France by Baghdadi et al. [83] and Fayad et al. [84].

5. Conclusions

Different approaches have been proposed for SSM estimation from space. The goal is to improve estimates by combining change detection logic with empirical or other approaches based on an ANN. The study is based on Sentinel-1 and Sentinel-2 data tested on the ISMN moisture network.

Relationships between temporal changes in radar signals and temporal changes in soil moisture are tested. Improved change detection relationships combine these effects with the contribution of vegetation through two optical and radar indices (*NDVI* and VH/VV ratio). The integration of the effect of vegetation slightly improves the precision with an *RMSE* that decreases slightly from 0.074 m^3/m^3 to 0.073 m^3/m^3 and 0.068 m^3/m^3 for VH/VV and *NDVI*, respectively.

Testing an ANN approach through numerous metrics based on radar and optical (VV, VH, VH/VV, *NDVI*, ΔVV, incidence angle, etc.) time series illustrates precision within a 0.08 m^3/m^3–0.09 (m^3/m^3) range. These results are greatly improved with the integration

as input of soil moisture estimated from the change detection approach. Thus, we move on to precision below the bar of 0.07 m^3/m^3 for the different possible combinations of metrics. Thus, it seems highly useful to propose this combination to improve the precision of the estimated soil moisture. Despite this improvement, there are some limitations at some stations, particularly related to the vegetation density and presence of forests or extreme climates with cold conditions. In the future, it would be very useful to propose a spatialization of this approach by considering auxiliary information of soil properties and land use for a better application of the proposed algorithms and improvement of proposed precision. In fact, this allows us to distinguish effects due more precisely to vegetation for which volume and attenuation scattering are different from one cover to another. For a high-resolution scale, this aspect, which is generally not considered for a low-resolution scale, seems important.

Author Contributions: S.N., E.A. and M.Z. developed methods and analyzed the data; all authors contributed to the materials/analysis tools; and M.Z. and E.A. wrote the paper. All authors have read and agreed to the published version of the manuscript.

Funding: This study was funded by Projects; ESA No. 4000126684/19/I-NB "ESA CCI+" and TAPAS TOSCA/CNES.

Data Availability Statement: The data presented in this study are available in International Soil Moisture Network (ISMN) https://ismn.geo.tuwien.ac.at/en/ and https://scihub.copernicus.eu/sites (accessed on 16 May 2022).

Acknowledgments: The authors thank the International Soil Moisture Network (ISMN) and the supporting networks for the availability of soil moisture data.

Conflicts of Interest: The authors declare no conflict of interest.

References

1. Koster, R.D.; Dirmeyer, P.A.; Guo, Z.; Bonan, G.; Chan, E.; Cox, P.; Gordon, C.T.; Kanae, S.; Kowalczyk, E.; Lawrence, D.; et al. Regions of Strong Coupling Between Soil Moisture and Precipitation. *Science* **2004**, *305*, 1138–1140. [CrossRef] [PubMed]
2. Anguela, T.P.; Zribi, M.; Hasenauer, S.; Habets, F.; Loumagne, C. Analysis of surface and root-zone soil moisture dynamics with ERS scatterometer and the hydrometeorological model SAFRAN-ISBA-MODCOU at Grand Morin watershed (France). *Hydrol. Earth Syst. Sci.* **2008**, *12*, 1415–1424. [CrossRef]
3. Albergel, C.; Zakharova, E.; Calvet, J.-C.; Zribi, M.; Pardé, M.; Wigneron, J.-P.; Novello, N.; Kerr, Y.; Mialon, A.; Fritz, N.-E. A first assessment of the SMOS data in southwestern France using in situ and airborne soil moisture estimates: The CAROLS airborne campaign. *Remote Sens. Environ.* **2011**, *115*, 2718–2728. [CrossRef]
4. Brocca, L.; Ciabatta, L.; Moramarco, T.; Ponziani, F.; Berni, N.; Wagner, W. Use of Satellite Soil Moisture Products for the Operational Mitigation of Landslides Risk in Central Italy. In *Satellite Soil Moisture Retrieval*; Elsevier: New York, NY, USA, 2016; Volume 7, pp. 231–247. [CrossRef]
5. Le Page, M.; Jarlan, L.; El Hajj, M.M.; Zribi, M.; Baghdadi, N.; Boone, A. Potential for the Detection of Irrigation Events on Maize Plots Using Sentinel-1 Soil Moisture Products. *Remote Sens.* **2020**, *12*, 1621. [CrossRef]
6. Ulaby, F.T.; Bradley, G.A.; Dobson, M.C. Microwave Backscatter Dependence on Surface Roughness, Soil Moisture, and Soil Texture: Part II-Vegetation-Covered Soil. *IEEE Trans. Geosci. Electron.* **1979**, *17*, 33–40. [CrossRef]
7. Jackson, T.J.; Cosh, M.H.; Bindlish, R.; Starks, P.J.; Bosch, D.D.; Seyfried, M.; Goodrich, D.C.; Moran, M.S.; Du, J.Y. Validation of Advanced Microwave Scanning Radiometer Soil Moisture Products. *IEEE Trans. Geosci. Remote Sens. Dec.* **2010**, *48*, 4256–4272. [CrossRef]
8. Kerr, Y.H.; Waldteufel, P.; Richaume, P.; Wigneron, J.-P.; Ferrazzoli, P.; Mahmoodi, A.; Al Bitar, A.; Cabot, F.; Gruhier, C.; Juglea, S.E.; et al. The SMOS Soil Moisture Retrieval Algorithm. *IEEE Trans. Geosci. Remote Sens.* **2012**, *50*, 1384–1403. [CrossRef]
9. Entekhabi, D.; Njoku, E.G.; O'Neill, P.E.; Kellogg, K.H.; Crow, W.T.; Edelstein, W.N.; Entin, J.K.; Goodman, S.D.; Jackson, T.J.; Johnson, J.; et al. The Soil Moisture Active Passive (SMAP) Mission. *Proc. IEEE* **2010**, *98*, 704–716. [CrossRef]
10. Kim, H.; Parinussa, R.; Konings, A.G.; Wagner, W.; Cosh, M.H.; Lakshmi, V.; Zohaib, M.; Choi, M. Global-scale assessment, and combination of SMAP with ASCAT (active) and AMSR2 (passive) soil moisture products. *Remote Sens. Environ.* **2018**, *204*, 260–275. [CrossRef]
11. Motte, E.; Zribi, M.; Fanise, P.; Egido, A.; Darrozes, J.; Al-Yaari, A.; Baghdadi, N.; Baup, F.; Dayau, S.; Fieuzal, R.; et al. GLORI: A GNSS-R Dual Polarization Airborne Instrument for Land Surface Monitoring. *Sensors* **2016**, *16*, 732. [CrossRef]
12. Colliander, A.; Reichle, R.; Crow, W.; Cosh, M.H.; Chen, F.; Chan, S.K.; Das, N.N.; Bindlish, R.; Chaubell, M.J.; Kim, S.; et al. Validation of Soil Moisture Data Products From the NASA SMAP Mission. *IEEE J. Sel. Top. Appl. Earth Obs. Remote Sens.* **2021**, *15*, 364–392. [CrossRef]

13. Wagner, W.; Bloeschl, G.; Pamaloni, P.; Calvet, J.C. Operational readiness of microwave remote sensing of soil moisture for hydrologic applications. *Nord. Hydrol.* **2007**, *38*, 1–20. [CrossRef]
14. Dorigo, W.; Wagner, W.; Albergel, C.; Albrecht, F.; Balsamo, G.; Brocca, L.; Chung, D.; Ertl, M.; Forkel, M.; Gruber, A.; et al. ESA CCI Soil Moisture for improved Earth system understanding: State-of-the art and future directions. *Remote Sens. Environ.* **2017**, *203*, 185–215. [CrossRef]
15. Moran, M.S.; Hymer, D.C.; Qi, J.; Sano, E.E. Soil moisture evaluation using multi-temporal synthetic aperture radar (SAR) in semiarid rangeland. *Agric. For. Meteorol.* **2000**, *105*, 69–80. [CrossRef]
16. Pierdicca, N.; Pulvirenti, L.; Bignami, C. Soil moisture estimation over vegetated terrains using multitemporal remote sensing data. *Remote Sens. Environ.* **2010**, *114*, 440–448. [CrossRef]
17. Bousbih, S.; Zribi, M.; Lili-Chabaane, Z.; Baghdadi, N.; El Hajj, M.; Gao, Q.; Mougenot, B. Potential of Sentinel-1 Radar Data for the Assessment of Soil and Cereal Cover Parameters. *Sensors* **2017**, *17*, 2617. [CrossRef]
18. Şekertekin, A.; Marangoz, A.M.; Abdikan, S. Soil Moisture Mapping Using Sentinel-1A Synthetic Aperture Radar Data. *Int. J. Environ. Geoinform.* **2018**, *5*, 178–188. [CrossRef]
19. Hajj, M.E.; Baghdadi, N.; Belaud, G.; Zribi, M.; Cheviron, B.; Courault, D.; Hagolle, O.; Charron, F. Irrigated Grassland Monitoring Using a Time Series of TerraSAR-X and COSMO-SkyMed X-Band SAR Data. *Remote Sens.* **2014**, *6*, 10002–10032. [CrossRef]
20. Srivastava, H.S.; Patel, P.; Sharma, Y.; Navalgund, R.R. Large-Area Soil Moisture Estimation Using Multi-Incidence-Angle RADARSAT-1 SAR Data. *IEEE Trans. Geosci. Remote Sens.* **2009**, *47*, 2528–2535. [CrossRef]
21. Balenzano, A.; Mattia, F.; Satalino, G.; Davidson, M.W.J. Dense Temporal Series of C- and L-band SAR Data for Soil Moisture Retrieval Over Agricultural Crops. *IEEE J. Sel. Top. Appl. Earth Obs. Remote Sens.* **2010**, *4*, 439–450. [CrossRef]
22. Ma, C.; Li, X.; McCabe, M.F. Retrieval of High-Resolution Soil Moisture through Combination of Sentinel-1 and Sentinel-2 Data. *Remote Sens.* **2020**, *12*, 2303. [CrossRef]
23. Wang, H.; Magagi, R.; Goita, K.; Jagdhuber, T. Refining a Polarimetric Decomposition of Multi-Angular UAVSAR Time Series for Soil Moisture Retrieval Over Low and High Vegetated Agricultural Fields. *IEEE J. Sel. Top. Appl. Earth Obs. Remote Sens.* **2019**, *12*, 1431–1450. [CrossRef]
24. Wang, H.; Magagi, R.; Goita, K.; Jagdhuber, T.; Hajnsek, I. Evaluation of Simplified Polarimetric Decomposition for Soil Moisture Retrieval over Vegetated Agricultural Fields. *Remote Sens.* **2016**, *8*, 142. [CrossRef]
25. Molero, B.; Merlin, O.; Malbeteau, Y.; Al Bitar, A.; Cabot, F.; Stefan, V.; Kerr, Y.; Bacon, S.; Cosh, M.; Bindlish, R.; et al. SMOS disaggregated soil moisture product at 1 km resolution: Processor overview and first validation results. *Remote Sens. Environ.* **2016**, *180*, 361–376. [CrossRef]
26. Kim, S.-B.; Moghaddam, M.; Tsang, L.; Burgin, M.; Xu, X.; Njoku, E.G. Models of L-Band Radar Backscattering Coefficients Over Global Terrain for Soil Moisture Retrieval. *IEEE Trans. Geosci. Remote Sens.* **2013**, *52*, 1381–1396. [CrossRef]
27. Kim, S.-B.; Van Zyl, J.J.; Johnson, J.T.; Moghaddam, M.; Tsang, L.; Colliander, A.; Dunbar, R.S.; Jackson, T.J.; Jaruwatanadilok, S.; West, R.; et al. Surface Soil Moisture Retrieval Using the L-Band Synthetic Aperture Radar Onboard the Soil Moisture Active–Passive Satellite and Evaluation at Core Validation Sites. *IEEE Trans. Geosci. Remote Sens.* **2017**, *55*, 1897–1914. [CrossRef]
28. Bousbih, S.; Zribi, M.; El Hajj, M.; Baghdadi, N.; Lili-Chabaane, Z.; Gao, Q.; Fanise, P. Soil Moisture and Irrigation Mapping in A Semi-Arid Region, Based on the Synergetic Use of Sentinel-1 and Sentinel-2 Data. *Remote Sens.* **2018**, *10*, 1953. [CrossRef]
29. Ezzahar, J.; Ouaadi, N.; Zribi, M.; Elfarkh, J.; Aouade, G.; Khabba, S.; Er-Raki, S.; Chehbouni, A.; Jarlan, L. Evaluation of Backscattering Models and Support Vector Machine for the Retrieval of Bare Soil Moisture from Sentinel-1 Data. *Remote Sens.* **2019**, *12*, 72. [CrossRef]
30. Notarnicola, C.; Angiulli, M.; Posa, F. Soil moisture retrieval from remotely sensed data: Neural network approach versus Bayesian method. *IEEE Trans. Geosci. Remote Sens.* **2008**, *46*, 547–557. [CrossRef]
31. El Hajj, M.; Baghdadi, N.; Zribi, M.; Bazzi, H. Synergic Use of Sentinel-1 and Sentinel-2 Images for Operational Soil Moisture Mapping at High Spatial Resolution over Agricultural Areas. *Remote Sens.* **2017**, *9*, 1292. [CrossRef]
32. Zribi, M.; Kotti, F.; Amri, R.; Wagner, W.; Shabou, M.; Chabaane, Z.L.; Baghdadi, N. Soil moisture mapping in a semiarid region, based on ASAR/Wide Swath satellite data. *Water Resour. Res.* **2014**, *50*, 823–835. [CrossRef]
33. Bauer-Marschallinger, B.; Freeman, V.; Cao, S.; Paulik, C.; Schaufler, S.; Stachl, T.; Modanesi, S.; Massari, C.; Ciabatta, L.; Brocca, L.; et al. Toward Global Soil Moisture Monitoring With Sentinel-1: Harnessing Assets and Overcoming Obstacles. *IEEE Trans. Geosci. Remote Sens.* **2018**, *57*, 520–539. [CrossRef]
34. Foucras, M.; Zribi, M.; Albergel, C.; Baghdadi, N.; Calvet, J.-C.; Pellarin, T. Estimating 500-m Resolution Soil Moisture Using Sentinel-1 and Optical Data Synergy. *Water* **2020**, *12*, 866. [CrossRef]
35. Gao, Q.; Zribi, M.; Escorihuela, M.J.; Baghdadi, N. Synergetic Use of Sentinel-1 and Sentinel-2 Data for Soil Moisture Mapping at 100 m Resolution. *Sensors* **2017**, *17*, 1966. [CrossRef]
36. Bazzi, H.; Baghdadi, N.; El Hajj, M.; Zribi, M.; Belhouchette, H. A Comparison of Two Soil Moisture Products S2MP and Copernicus-SSM over Southern France. *IEEE J. Sel. Top. Appl. Earth Obs. Remote Sens.* **2019**, *100*, 10–18. [CrossRef]
37. Dorigo, W.A.; Wagner, W.; Hohensinn, R.; Hahn, S.; Paulik, C.; Xaver, A.; Gruber, A.; Drusch, M.; Mecklenburg, S.; van Oevelen, P.; et al. The International Soil Moisture Network: A data hosting facility for global in situ soil moisture measurements. *Hydrol. Earth Syst. Sci.* **2011**, *15*, 1675–1698. [CrossRef]

38. Cappelaere, C.; Descroix, L.; Lebel, T.; Boulain, N.; Ramier, D.; Laurent, J.-P.; Le Breton, E.; Boubkraoui, S.; Bouzou Moussa, I.; Quantin, G.; et al. The AMMA Catch observing system in the cultivated Sahel of Southwest Niger- Strategy, Implementation and Site conditions. *J. Hydrol.* **2009**, *375*, 34–51. [CrossRef]
39. de Rosnay, P.; Gruhier, C.; Timouk, F.; Baup, F.; Mougin, E.; Hiernaux, P.; Kergoat, L.; LeDantec, V. Multi-scale soil moisture measurements at the Gourma meso-scale site in Mali. *J. Hydrol.* **2009**, *375*, 241–252. [CrossRef]
40. Lebel, T.; Cappelaere, B.; Galle, S.; Hanan, N.; Kergoat, L.; Levis, S.; Vieux, B.; Descroix, L.; Gosset, M.; Mougin, E.; et al. AMMA-CATCH studies in the Sahelian region of West-Africa: An overview. *J. Hydrol.* **2009**, *375*, 3–13. [CrossRef]
41. Galle, S.; Grippa, M.; Peugeot, C.; Moussa, I.B.; Cappelaere, B.; Demarty, J.; Mougin, E.; Panthou, G.; Adjomayi, P.; Agbossou, E.; et al. AMMA-CATCH, a Critical Zone Observatory in West Africa Monitoring a Region in Transition. *Vadose Zone J.* **2018**, *17*, 1–24. [CrossRef]
42. Mougin, E.; Hiernaux, P.; Kergoat, L.; Grippa, M.; de Rosnay, P.; Timouk, F.; Le Dantec, V.; Demarez, V.; Lavenu, F.; Arjounin, M.; et al. The AMMA-CATCH Gourma observatory site in Mali: Relating climatic variations to changes in vegetation, surface hydrology, fluxes and natural resources. *J. Hydrol.* **2009**, *375*, 14–33. [CrossRef]
43. Pellarin, T.; Laurent, J.; Cappelaere, B.; Decharme, B.; Descroix, L.; Ramier, D. Hydrological modelling and associated microwave emission of a semi-arid region in South-western Niger. *J. Hydrol.* **2009**, *375*, 262–272. [CrossRef]
44. Musial, J.P.; Dabrowska-Zielinska, K.; Kiryla, W.; Oleszczuk, R.; Gnatowski, T.; Jaszczynski, J. Derivation and validation of the high-resolution satellite soil moisture products: A case study of the biebrza sentinel-1 validation sites. *Geoinf. Issues* **2016**, *8*, 37–53.
45. Zreda, M.; Desilets, D.; Ferré Ty, P.A.; Scott, R.L. Measuring soil moisture content non-invasively at intermediate spatial scale using cosmic-ray neutrons. *Geophys. Res. Lett.* **2008**, *35*, 1–5. [CrossRef]
46. Zreda, M.; Shuttleworth, W.J.; Zeng, X.; Zweck, C.; Desilets, D.; Franz, T.; Rosolem, R. COSMOS: The COsmic-ray Soil Moisture Observing System. *Hydrol. Earth Syst. Sci.* **2012**, *16*, 4079–4099. [CrossRef]
47. Jensen, K.H.; Refsgaard, J.C. HOBE: The Danish Hydrological Observatory. *Vadose Zone J.* **2018**, *17*, 1–24. [CrossRef]
48. Bircher, S.; Skou, N.; Jensen, K.H.; Walker, J.P.; Rasmussen, L. A soil moisture and temperature network for SMOS validation in Western Denmark. *Hydrol. Earth Syst. Sci.* **2012**, *16*, 1445–1463. [CrossRef]
49. Al-Yaari, A.; Dayau, S.; Chipeaux, C.; Aluome, C.; Kruszewski, A.; Loustau, D.; Wigneron, J.-P. The AQUI Soil Moisture Network for Satellite Microwave Remote Sensing Validation in South-Western France. *Remote Sens.* **2018**, *10*, 1839. [CrossRef]
50. Wigneron, J.-P.; Dayan, S.; Kruszewski, A.; Aluome, C.; Al-Yaari, A.; Fan, L.; Guven, S.; Chipeaux, C.; Moisy, C.; Guyon, D.; et al. The aqui network: Soil moisture sites in the "les landes" forest and graves vineyards (Bordeaux Aquitaine region, France). In Proceedings of the IGARSS 2018-2018 IEEE International Geoscience and Remote Sensing Symposium, Valencia, Spain, 22–27 July 2018; pp. 3739–3742.
51. Zappa, L.; Forkel, M.; Xaver, A.; Dorigo, W. Deriving Field Scale Soil Moisture from Satellite Observations and Ground Measurements in a Hilly Agricultural Region. *Remote Sens.* **2019**, *11*, 2596. [CrossRef]
52. Xaver, A.; Zappa, L.; Rab, G.; Pfeil, I.; Vreugdenhil, M.; Hemment, D.; Dorigo, W.A. Evaluating the suitability of the consumer low-cost Parrot Flower Power soil moisture sensor for scientific environmental applications. *Geosci. Instrum. Methods Data Syst.* **2020**, *9*, 117–139. [CrossRef]
53. Zappa, L.; Woods, M.; Hemment, D.; Xaver, A.; Dorigo, W. Evaluation of remotely sensed soil moisture products using crowdsourced measurements. In Proceedings of the Eighth international conference on remote sensing and geoinformation of the environment (RSCy2020), Paphos, Cyprus, 26 August 2020; Volume 11524, p. 115241U. [CrossRef]
54. Vreugdenhil, M.; Dorigo, W.; Broer, M.; Haas, P.; Eder, A.; Hogan, P.; Blöschl, G.; Wagner, W. Towards a high-density soil moisture network for the validation of SMAP in Petzenkirchen, Austria. In Proceedings of the 2013 IEEE International Geoscience and Remote Sensing Symposium-IGARSS, Melbourne, VIC, Australia, 21–26 July 2013; pp. 1865–1868. [CrossRef]
55. Blöschl, G.; Blaschke, A.P.; Broer, M.; Bucher, C.; Carr, G.; Chen, X.; Eder, A.; Exner-Kittridge, M.; Farnleitner, A.; Flores-Orozco, A.; et al. The Hydrological Open Air Laboratory (HOAL) in Petzenkirchen: A hypothesis-driven observatory. *Hydrol. Earth Syst. Sci.* **2016**, *20*, 227–255. [CrossRef]
56. Alday, J.G.; Camarero, J.J.; Revilla, J.; De Dios, V.R. Similar diurnal, seasonal and annual rhythms in radial root expansion across two coexisting Mediterranean oak species. *Tree Physiol.* **2020**, *40*, 956–968. [CrossRef] [PubMed]
57. Su, Z.; Wen, J.; Dente, L.; van der Velde, R.; Wang, L.; Ma, Y.; Yang, K.; Hu, Z. The Tibetan Plateau observatory of plateau scale soil moisture and soil temperature (Tibet-Obs) for quantifying uncertainties in coarse resolution satellite and model products. *Hydrol. Earth Syst. Sci.* **2011**, *15*, 2303–2316. [CrossRef]
58. Dente, L.; Su, Z.; Wen, J. Validation of SMOS Soil Moisture Products over the Maqu and Twente Regions. *Sensors* **2012**, *12*, 9965–9986. [CrossRef] [PubMed]
59. Beyrich, F.; Adam, W.K. Site and Data Report for the Lindenberg Reference Site in CEOP—Phase 1. *Berichte des Deutschen Wetterdienstes* **2007**, *230*. Offenbach am Main.
60. Su, Z.; de Rosnay, P.; Wen, J.; Wang, L.; Zeng, Y. Evaluation of ECMWF's soil moisture analyses using observationson the Tibetan Plateau. *J. Geophys. Res. Atmos.* **2013**, *118*, 5304–5318. [CrossRef]
61. Canisius, F. *Calibration of Casselman, Ontario Soil Moisture Monitoring Network*; Agriculture and Agri-Food: Ottawa, ON, Canada, 2011; 37p.
62. L'Heureux, J. Installation Report for AAFC-SAGES Soil Moisture Stations in Kenaston, SK. In *Calibration of Casselman, Ontario Soil Moisture Monitoring Network*; Agriculture and Agri-Food: Ottawa, ON, Canada, 2011; 37p.

63. Ojo, E.R.; Bullock, P.R.; L'Heureux, J.; Powers, J.; McNairn, H.; Pacheco, A. Calibration and Evaluation of a Frequency Domain Reflectometry Sensor for Real-Time Soil Moisture Monitoring. *Vadose Zone J.* **2015**, *14*. [CrossRef]
64. Gonzalez-Zamora, A.; Sanchez, N.; Pablos, M.; Martinez-Fernandez, J. Cci soil moisture assessment with SMOS soil moisture and in situ data under different environmental conditions and spatial scales in Spain. *Remote Sens. Environ.* **2018**, *225*, 469–482. [CrossRef]
65. Schaefer, G.; Cosh, M.; Jackson, T. The usda natural resources conservation service soil climate analysis network (scan). *J. Atmos. Ocean. Technol.* **2007**, *24*, 2073–2077. [CrossRef]
66. Calvet, J.-C.; Fritz, N.; Froissard, F.; Suquia, D.; Petitpa, A.; Piguet, B. In situ soil moisture observations for the CAL/VAL of SMOS: The SMOSMANIA network. In Proceedings of the 2007 IEEE International Geoscience and Remote Sensing Symposium, Barcelona, Spain, 23–28 July 2007; pp. 1196–1199. [CrossRef]
67. Albergel, C.; Rüdiger, C.; Pellarin, T.; Calvet, J.-C.; Fritz, N.; Froissard, F.; Suquia, D.; Petitpa, A.; Piguet, B.; Martin, E. From near-surface to root-zone soil moisture using an exponential filter: An assessment of the method based on in situ observations and model simulations. *Hydrol. Earth Syst. Sci.* **2008**, *12*, 1323–1337. [CrossRef]
68. Calvet, J.-C.; Fritz, N.; Berne, C.; Piguet, B.; Maurel, W.; Meurey, C. Deriving pedotransfer functions for soil quartz fraction in southern france from reverse modeling. *Soil* **2016**, *2*, 615–629. [CrossRef]
69. Leavesley, G.H.; David, O.; Garen, D.C.; Lea, J.; Marron, J.K.; Pagano, T.C.; Strobel, M.L. A modeling framework for improved agricultural water supply forecasting. In *AGU Fall Meeting Abstracts*; American Geophysical Union: Washington, DC, USA, 2008; Volume 2008, pp. C21A–0497.
70. Zacharias, S.; Bogena, H.; Samaniego, L.; Mauder, M.; Fuß, R.; Pütz, T.; Frenzel, M.; Schwank, M.; Baessler, C.; Butterbach-Bahl, K.; et al. A Network of Terrestrial Environmental Observatories in Germany. *Vadose Zone J.* **2011**, *10*, 955–973. [CrossRef]
71. Bogena, H.; Kunkel, R.; Pütz, T.; Vereecken, H.; Kruger, E.; Zacharias, S.; Dietrich, P.; Wollschläger, U.; Kunstmann, H.; Papen, H.; et al. Tereno-long-term monitoring network for terrestrial environmental research. *Hydrol. Und Wasserbewirtsch.* **2012**, *56*, 138–143.
72. Bogena, H.R. Tereno: German network of terrestrial environmental observatories. *J. Large-Scale Res. Facil. JLSRF* **2016**, *2*, 52. [CrossRef]
73. Bell, J.E.; Palecki, M.A.; Baker, C.B.; Collins, W.G.; Lawrimore, J.H.; Leeper, R.; Hall, M.E.; Kochendorfer, J.; Meyers, T.P.; Wilson, T.; et al. U.S. Climate Reference Network Soil Moisture and Temperature Observations. *J. Hydrometeorol.* **2013**, *14*, 977–988. [CrossRef]
74. Schwerdt, M.; Schmidt, K.; Tous Ramon, N.; Klenk, P.; Yague-Martinez, N.; Prats-Iraola, P.; Zink, M.; Geudtner, D. Independent system calibration of Sentinel-1B. *Remote Sens.* **2017**, *9*, 511. [CrossRef]
75. Hagolle, O.; Huc, M.; Villa Pascual, D.; Dedieu, G. A Multi-Temporal and Multi-Spectral Method to Estimate Aerosol Optical Thickness over Land, for the Atmospheric Correction of FormoSat-2, LandSat, VENμS and Sentinel-2 Images. *Remote Sens.* **2015**, *7*, 2668–2691. [CrossRef]
76. Wagner, W.; Lemoine, G.; Rott, H. A method for estimating soil moisture from ERS Scatterometer and soil data. *Remote Sens. Environ.* **1999**, *70*, 191–207. [CrossRef]
77. Pellarin, T.; Calvet, J.C.; Wagner, W. Evaluation of ERS scatterometer soil moisture products over a half-degree region in southwestern France. *Geophys. Res. Lett.* **2006**, *33*, 1–6. [CrossRef]
78. Zribi, M.; André, C.; Decharme, B. A method for soil moisture estimation in Western Africa based on ERS Scatter meter. *IEEE Trans. Geosci. Remote Sens.* **2008**, *46*, 438–448. [CrossRef]
79. ASCE Task Committee on Application of Artificial Neural Networks in Hydrology. Artificial neural networks in hydrology. I: Preliminary concepts. *J. Hydrol. Eng.* **2000**, *5*, 115–123. [CrossRef]
80. Tanty, T.S.D.R.; Desmukh, T.; Bhopal, M. Application of Artificial Neural Network in Hydrology—A Review. *Int. J. Eng. Res.* **2015**, *V4*, 184–188. [CrossRef]
81. Veloso, A.; Mermoz, S.; Bouvet, A.; Le Toan, T.; Planells, M.; Dejoux, J.F.; Ceschia, E. Understanding the temporal behavior of crops using Sentinel-1 and Sentinel-2-like data for agricultural applications. *Remote Sens. Environ.* **2017**, *199*, 415–426. [CrossRef]
82. Baghdadi, N.; Zribi, M. *Land Surface Remote Sensing in Continental Hydrology*; ISTE Press: London, UK; Elsevier: Oxford, UK, 2016; ISBN 9781785481048.
83. Baghdadi, N.; Bazzi, H.; El Hajj, M.; Zribi, M. Detection of Frozen Soil Using Sentinel-1 SAR Data. *Remote Sens.* **2018**, *10*, 1182. [CrossRef]
84. Fayad, I.; Baghdadi, N.; Bazzi, H.; Zribi, M. Near Real-Time Freeze Detection over Agricultural Plots Using Sentinel-1 Data. *Remote Sens.* **2020**, *12*, 1976. [CrossRef]